Supporting Information

A simple strategy generating hydrothermally stable core-shell platinum catalysts with tunable distribution of acid sites

Houlin Wang,[a,1] Minghan Liu,[b,1] Yue Ma,[b] Ke Gong,[a] Wei Liu,[a] Rui Ran,[b] Duan Weng,[b] Xiaodong Wu,*[,b] and Shuang Liu*[,a]

[a] *School of Materials Science and Engineering, Ocean University of China, Qingdao 266100, China.*

[b] *The Key Laboratory of Advanced Materials of Ministry of Education, School of Materials Science and Engineering, Tsinghua University, Beijing 100084, China*

[1]*Contributed equally to this work.*

Correspondence to:

* lius@ouc.edu.cn (S. Liu)

* wuxiaodong@ ouc.edu.cn (X. Wu)

Table of Contents:

Supplementary instruction for the characterizations:

(1) CO titration

CO titration experiments were conducted on the same apparatus to that used in NO-TPO and C_3H_8-TPO tests via a method as described in ref. (1). Prior to the test, about 30 mg of catalyst (pre-reduced at 350 °C in hydrogen for 30 min) was treated in 30% O_2/N_2 (300 ml/min) at room temperature for 1 h. The flow was then switched to N_2 (300 ml/min), and the reactor temperature was heated up to 150 °C. At this titration temperature, the flow was changed to 1% CO/N_2 (100 ml/min), and the outlet CO_2 concentration was monitored by an infrared spectrometer (MKS Multigas 2030). The CO_2 trace was followed until it decreased to below the detection limit.

CO can titrate the oxygen monolayer completely from Pt at 150 °C through a reaction stoichiometry $CO+O–Pt_s \rightarrow CO_2+Pt_s$.[1] Therefore, the number of exposed Pt atoms (Pt_s) should equal to that of the CO_2 generated (or the atomic oxygen removed). Corresponding quantitative results were shown in Table S1.

Furthermore, in order to give accurate comparison of different catalysts by excluding the influence of Pt content, CO_2 production curves normalized by Pt contents of different catalysts were illustrated in Figure 3C.

(2) Ammonia temperature–programmed desorption (NH_3-TPD)

The NH_3-TPD tests were performed on a Micromeritics AutoChem II 2920 with a TCD detector. Prior to the test, about 50 mg of pre-reduced catalyst was treated in helium (100 mL/min) at 500 °C for 30 min for proper degassing. Then it was exposed in 1000 ppm NH_3/He (100 mL/min) at 100 °C for 30 min then flushed by He (100 mL/min). Afterwards, the NH_3 desorption profiles were obtained by heating the reactor to 500 °C at a ramp rate of 10 °C/min in a helium stream (100 mL/min). Corresponding quantitative results were shown in Table S2.

(3) Diffuse reflectance infrared Fourier transform (DRIFT) spectra of NH_3 adsorption

DRIFT spectra were measured on a FT-IR spectrometer (Thermo Nicolet 6700) using a

heatable environmental reaction cell with ZnSe windows, which was connected to a gas-dosing system. Prior to the test, pre-reduced catalyst was treated in nitrogen (100 mL/min) at 500 °C for 30 min for proper degassing. Afterwards, the reaction cell was cooled down to 100 °C, the spectrum was then collected and used as the background. A gas flow containing 1000 ppm NH_3/N_2 (100 mL/min) was then introduced. After saturated with ammonia (30 min), the gas flow was switched to nitrogen (100 mL/min) and flushed for another 30 min. The spectra were then recorded and converted via Nicolet OMNIC™ software (Ver. 7.3) into Kubelka–Munk units (Figure S5).

(4) Diffuse reflectance infrared Fourier transform (DRIFT) spectra of C_3H_8 adsorption

DRIFT spectra of C_3H_8 adsorption were measured by a similar process on the same apparatus to that used in NH_3 adsorption, except that a gas flow containing 800 ppm C_3H_8/N_2 (100 mL/min) was applied. The spectra were shown in Figure 5D.

Supplementary instruction for TOF calculation:

The turnover frequency values for NO and C_3H_8 conversion were calculated based on the NO_2 formation and C_3H_8 consumption in the steady-state measurements, respectively:

$$\mathrm{TOF_{NO}} = \frac{[\mathrm{NO_2}]_{\mathrm{out}} \times V_{gas}}{m_{cat} \times [\mathrm{Pt_s}]} \ [\mathrm{h^{-1}}] \qquad \mathrm{TOF_{C_3H_8}} = \frac{([\mathrm{C_3H_8}]_{\mathrm{in}} - [\mathrm{C_3H_8}]_{\mathrm{out}}) \times V_{gas}}{m_{cat} \times [\mathrm{Pt_s}]} \ [\mathrm{h^{-1}}]$$

where V_{gas}: total molar flow rate during reactions, $m_{cat.}$: mass of catalyst in the reactor bed for each reaction (~50 mg) and $[Pt_s]$: amount of actual exposed Pt atoms obtained from CO titration ($mmol/g_{catalyst}$, see Table S1).

Supplementary tables:

Table S1. Summary of structure data of the catalysts.

Catalyst	S_{BET} (m^2/g) [a]	Average Pt particle size (nm) [b]	Exposed Pt atom (mmol/$g_{catalyst}$) [c]	Si/Al ratio [d]	Pt content (%) [d]
Pt@Si	198	5.6	0.64		27.4
Pt@SiAl	122	5.5	0.40	9.2:1	25.3
Pt@Si@SiAl	134	5.6	0.49	8.6:1	25.2
Pt@Si-A	83	33.7	0.01		
Pt@SiAl-A	107	6.5	0.12		
Pt@Si@SiAl-A	102	7.6	0.09		

[a] Obtained from N_2 physisorption at -196 ºC.

[b] Calculated by Scherrer equation from the XRD data.

[c] Obtained from CO titration tests.

[d] Obtained from ICP results.

Table S2. Summary of acidity properties of the catalysts.

Catalyst	Total NH_3 desorption (μmol/g cat.) [a]	NH_3 desorption at relatively high temperatures (μmol/g cat.) [b]
Pt@Si	69.8	17.4
Pt@SiAl	106.6	42.4
Pt@Si@SiAl	130.6	42.9
Pt@Si-A	11.2	3.9
Pt@SiAl-A	57.6	33.7
Pt@Si@SiAl-A	66.0	25.1

[a] Calculated from the total NH_3 desorbed in NH_3–TPD.

[b] Calculated from area of the orange peaks in Figure S3.

Table S3. Summary of catalytic performance of the catalysts.

Catalyst	NO conversion at 185 ºC (%) [a]	T_{50} for C_3H_8 oxidation (ºC) [b]	NO oxidation TOF at 80 ºC/100 ºC [c]	C_3H_8 oxidation TOF at 150 ºC/170 ºC [d]
Pt@Si	68.1	364	4.2/7.1	0.6/1.0
Pt@SiAl	89.5	218	6.5/9.9	1.7/3.9
Pt@Si@SiAl	67.5	260	4.1/7.2	1.2/2.1
Pt@Si-A	9.4	> 500		
Pt@SiAl-A	65.8	229		
Pt@Si@SiAl-A	52.1	295		

[a] Obtained from NO temperature-programmed oxidation (NO-TPO) tests.

[b] Temperatures at which 50% of C_3H_8 was oxidized to CO_2. Obtained from C_3H_8-TPO tests.

[c] Obtained from the steady-state NO oxidation tests. Units in 10^{-4} s^{-1} per exposed Pt atom.

[d] Obtained from the steady-state C_3H_8 oxidation tests. Units in 10^{-4} s^{-1} per exposed Pt atom.

Supplementary figures:

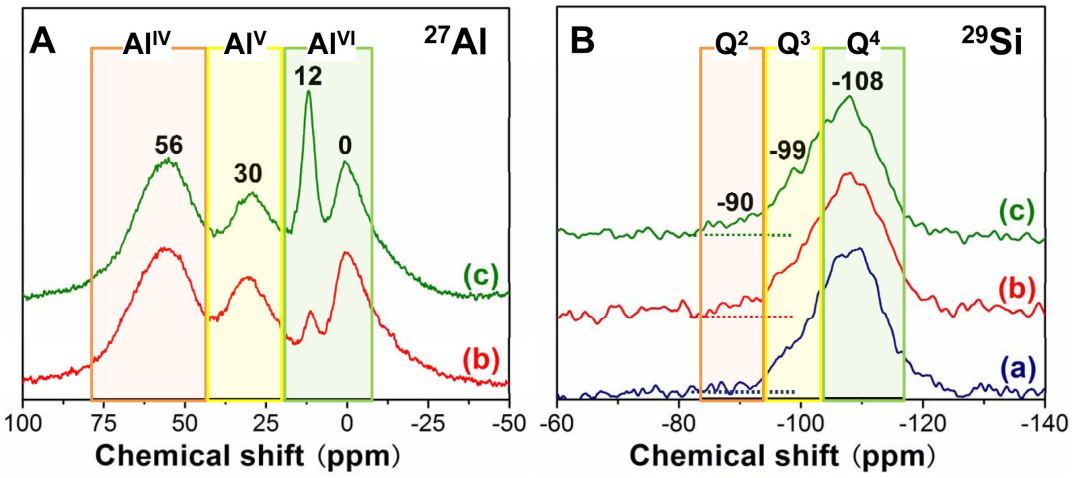

Figure S1. (A) ^{27}Al and (B) ^{29}Si NMR spectra of (a) Pt@Si, (b) Pt@SiAl and (c) Pt@Si@SiAl.

For ^{27}Al NMR spectra, the bands at around 80~40, 40~20 and 20~-5 ppm were assigned to four-, five- and six-coordinated Al species, respectively.[2] Specifically, the signal at 12 ppm and 0 ppm came from Al^{VI} in isolated and agglomerated hydrolyzed aluminum ions, respectively.[3] Given that most of the aluminum species were confined over the surface of Pt@Si@SiAl, it is reasonable that this catalyst possessed more aggregated aluminum oxides than Pt@SiAl. Notably, both the catalysts demonstrated a high content of Al^{IV}, which was closely related with the formation of Brønsted acid sites.[3,4]

As for ^{29}Si NMR spectra, the bands centered at -108, -99 and -90 can be attributed to ^{29}Si with Q^4 coordination (four Si atoms in the second coordination sphere), Q^3- and Q^2-type silicon sites (three and two Si atoms, others as H or Al atoms in the second coordination sphere), respectively.[3,4] By comparing Q^2 fractions of the three curves in Figure S1-B, it is clearly that aluminum was built into the aluminosilica phase of both Pt@SiAl and Pt@Si@SiAl.

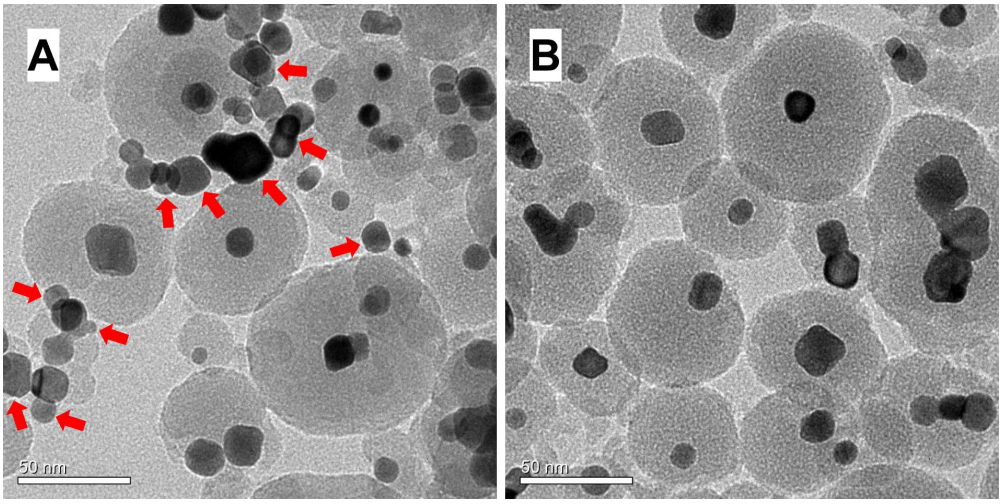

Figure S2. Typical TEM images of (A) Pt@Si and (B) Pt@SiAl after refluxing in distilled water at 100 ℃ for 24h (water-to-sample ratio: 1 L/g). The "naked" Pt particles without outer shell were labeled with red arrows. It is clearly that the former catalyst experienced severe dissolution of the silica shell, while the latter one remained a core-shell structure.

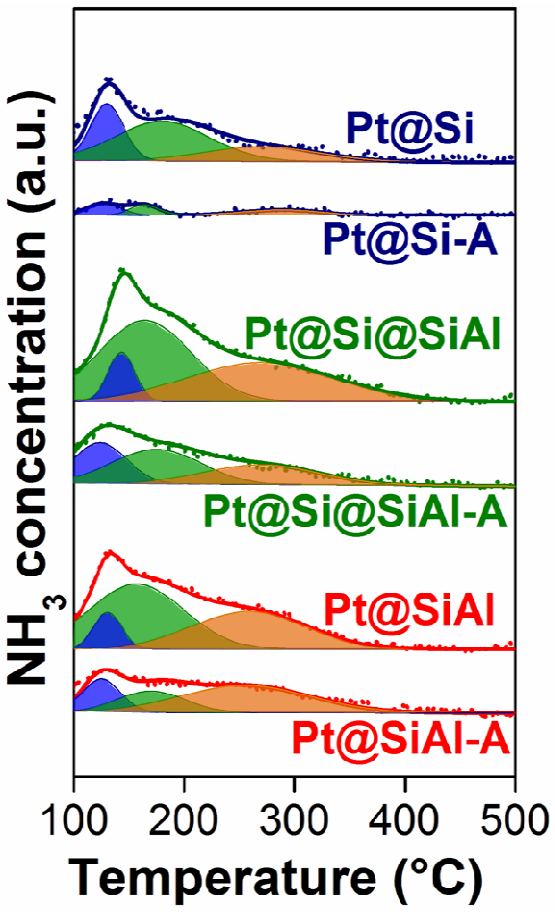

Figure S3. Gaussian deconvolution of the NH_3-TPD profiles.

The low-temperature peaks (blue: 100~170°C; green: 100~250°C) may be attributed to ammonia adsorbed on weak Lewis/Brønsted acid sites, while the high-temperature one (orange: 160~400°C) came from ammonia adsorbed on medium Brønsted acid sites.[5] Corresponding quantized NH_3 desorption amounts were listed detailedly in Table S2.

According to the correlation given by Yori et al.,[6] the NH_3 species desorbed at relatively high temperature (160~400°C) is related with acid sites with strength of H_0 = -8.1~-15.5 (average of ~-12.0). Based on the results obtained by Yoshida et al.[7] and Kobayashi et al.[8], this acid strength change is strong enough to affect the electronic states of Pt significantly.

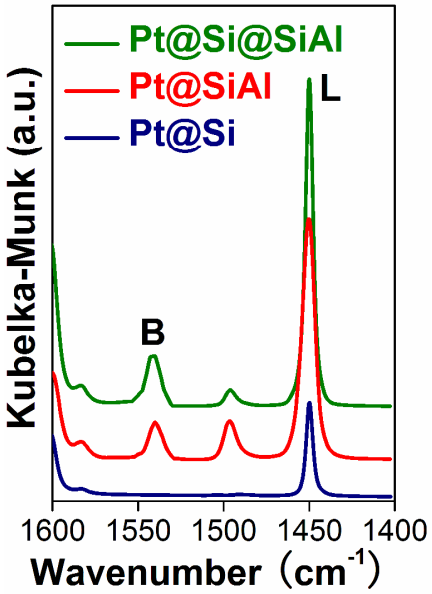

Figure S4. IR spectra of pyridine adsorption. All the samples were initially outgassed at 500°C for 1 h. Spectra were recorded at room temperature, after admission of pyridine, adsorption at room temperature and evacuation at 150°C (units in Kubelka–Munk).

Brønsted (B) and Lewis (L) acid sites are observed at around 1540 and 1450 cm^{-1}, respectively.[5] It is clearly that Pt@Si possessed much fewer Brøsted and Lewis acid sites compared with Pt@Si@SiAl and Pt@SiAl.

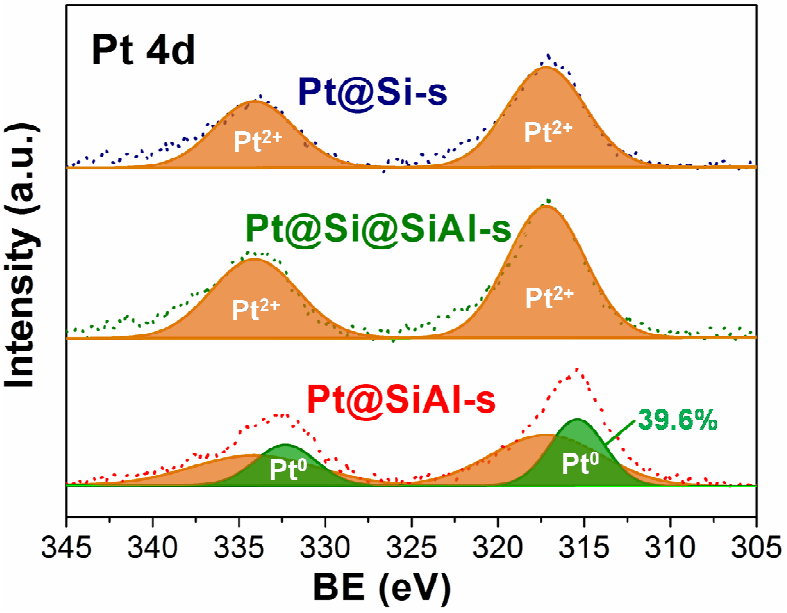

Figure S5. Gaussian deconvolution of the Pt 4d XPS spectra.

The bands centered at 317.2 and 315.4 eV were attributed to Pt^{2+} and Pt^0, respectively.[9] Obviously, all of the surface platinum species over Pt@Si-s and Pt@Si@SiAl-s converted into PtO_x, while 39.6% of the surface platinum on Pt@SiAl-s remained as metallic Pt^0.

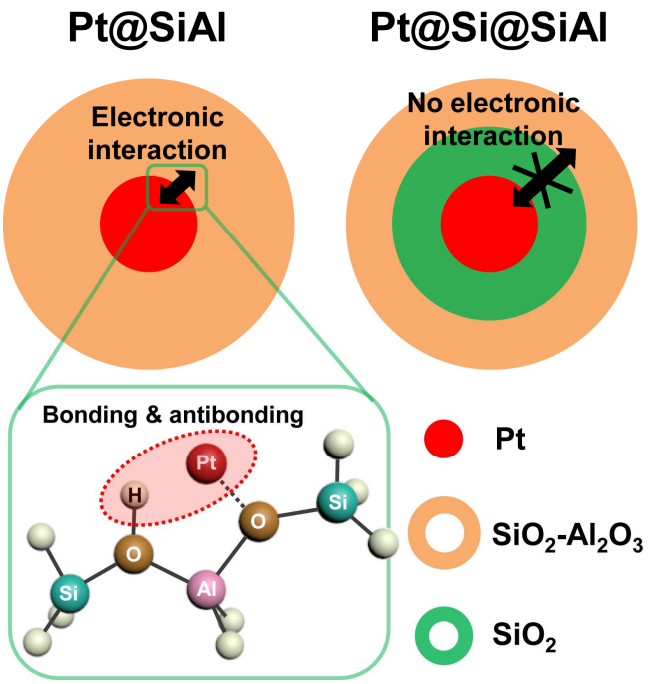

Figure S6. Scheme of the Pt-acid site electronic interactions in Pt@SiAl and Pt@Si@SiAl.

Detailed information about the electronic interaction between Pt atoms and Brønsted protons can be found in ref. (10).

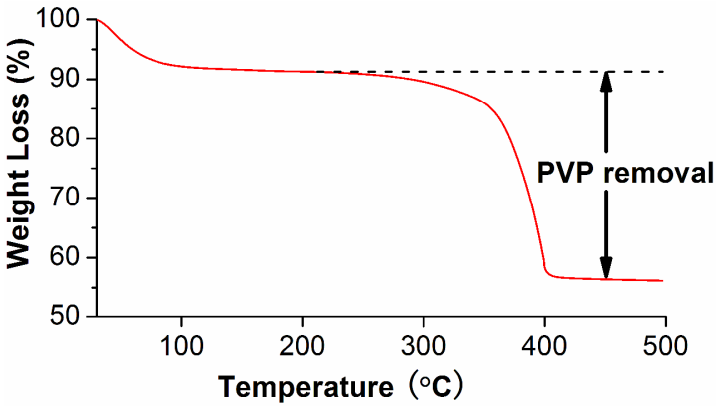

Figure S7. Weight loss curve of PVP-stabilized Pt@SiO_2 during temperature-programmed oxidation in air (ramp rate = 2 °C/min).

Obviously, all of the carbonaceous capping agent (PVP) can be removed effectively at temperatures below 500 °C. This means that no residual of capping agent was expected for the catalysts (calcined at 500 °C for hours) studied in this work.

References:

(1) Pazmiño, J.; Miller, J.; Mulla, S.; Delgass, W.; Ribeiro, F. Kinetic Studies of the Stability of Pt for NO Oxidation: Effect of Sulfur and Long-term Aging. *J. Catal.* **2011**, *282*, 13−24.

(2) Haouas, M.; Taulelle, F.; Martineau, C. Recent Advances in Application of ^{27}Al NMR Spectroscopy to Materials Science. *Prog. Nucl. Mag. Res. Sp*. **2016**, *94−95*, 11−36.

(3) Hensen, E.; Poduval, D.; Magusin, P.; Coumans, A.; van Veen, J. Formation of Acid Sites in Amorphous Silica-alumina. *J. Catal.* **2010**, *269*, 201−218.

(4) Lang, S.; Benz, M.; Obenaus, U.; Himmelmann, R.; Scheibe, M.; Klemm, E.; Weitkamp, J.; Hunger, M. Mechanisms of the $AlCl_3$ Modification of Siliceous Microporous and Mesoporous Catalysts Investigated by Multi-Nuclear Solid-State NMR. *Top. Catal.* **2017**, *60*, 1537−1553.

(5) Na, K.; Alayoglu, S.; Ye, R.; Somorjai, G. A. Effect of Acidic Properties of Mesoporous Zeolites Supporting Pt Nanoparticles on Hydrogenative Conversion of Methylcyclopentane. *J. Am. Chem. Soc*. **2014**, *136*, 17207−17212.

(6) Yori, J. C.; Krasnogor, L. M.; Castro, A. A. Correlation Between Acid Strength (H_o) and Ammonia Desorption Temperature for Aluminas and Silica-Aluminas. *React. Kinet. Catal. Lett.* **1986**, *32*, 27−32.

(7) Yazawa, Y.; Takagi, N.; Yoshida, H.; Komai, S.; Satsuma, A.; Tanaka, T.; Yoshida, S.; Hattori, T. The Support Effect on Propane Combustion over Platinum Catalyst: Control of the Oxidation-resistance of Platinum by the Acid Strength of Support Materials. *Appl. Catal., A* **2002**, *233*, 103−112.

(8) Kobayashi, M.; Morita, A.; Ikeda, M. The Support Effect in Oxidizing Atmosphere on Propane Combustion over Platinum Supported on TiO_2, TiO_2–SiO_2 and TiO_2–SiO_2–WO_3. *Appl. Catal., B* **2007**, *71*, 94−100.

(9) Corroa, G.; Cano, C.; Fierro, J. A Study of Pt–Pd/γ-Al_2O_3 Catalysts for Methane Oxidation Resistant to Deactivation by Sulfur Poisoning. *J. Mol. Catal. A* **2010**, *315*, 35−42.

(10) Treesukol, P.; Srisuk, K.; Limtrakul, J.; Truong, T. N. Nature of the Metal-Support Interaction in Bifunctional Catalytic Pt/H-ZSM-5 Zeolite. *J. Phys. Chem. B* **2005,** *109*, 11940−11945.